JOURNAL OF APPLIED ELECTROCHEMISTRY 17 (1987) 1083–1092

Triangular potential sweep voltammetric study of porous iron electrodes in alkali solutions

G. PARUTHIMAL KALAIGNAN, V. S. MURALIDHARAN, K. I. VASU

Central Electrochemical Research Institute, Karaikudi 623006, India

Received 24 April 1986; revised 9 April 1987

The cyclic voltammograms of pure iron and sintered iron electrodes in 6.0 M KOH solutions revealed a plateau and two anodic peaks in the forward direction and two cathodic peaks in the backward direction when polarized from −1.3 to −0.3 V vs Hg/HgO. In the forward scan the formation of $Fe(OH)_2$ and FeOOH occurs and these are subsequently reduced to $Fe(OH)_2$ and iron in the backward scan. The peak potential separation of the Fe/Fe(II) and Fe(II)/Fe(III) couples at zero sweep rate and the ratio of cathodic to anodic charges at zero sweep rates for the above two redox couples have been used to evaluate the reversibility of porous iron electrodes. Additions of LiOH, Na_2S, FeS, sulphur, Sb_2O_3 and As_2O_3 on the reversibility of these redox couples have been discussed. A suitable electrode fabrication condition has been suggested.

1. Introduction

Porous iron electrodes have been the subject of theoretical and practical investigations because of their use in alkaline batteries (iron–air and nickel–iron systems). From the discharge studies in 5 M KOH solutions it appears that most of the metal is oxidized to $Fe(OH)_2$ at the first discharge plateau and the second plateau is due to the mixture of FeOOH and Fe_3O_4 [1–3]. Scanning electron microscopic studies revealed the formation of $Fe(OH)_2$ during the first discharge. On continuous discharge, the product on the electrodes became a sludge, probably of FeOOH [4]. Mössbauer spectroscopy identified the phases *in situ* during the cyclic galvanostatic oxidation and reduction of iron. The first anodic arrest is due to $Fe(OH)_2$ and the second is due to β-FeOOH and unreacted $Fe(OH)_2$ [5, 6]. The formation of soluble Fe(II) and Fe(III) species [7, 8] has been identified using a gold ring and iron disc systems. Single and repetitive cyclic voltammetry was employed earlier for solid and porous electrodes in higher alkali concentrations and at higher temperatures [9–12]. The effect of lithium ion, sulphide ion and FeO has been studied for solid electrodes [13–15]. This paper deals with polarization characteristics of solid and porous iron electrodes in alkali solutions and the effect of additives on the reversibility of the electrode processes.

2. Experimental details

2.1. *Solid electrode*

The electrodes were prepared from pure iron sheets (99.95% Fe, 0.025% C, 0.0056% Mn, 0.011% S) and made into discs of 1.0 cm^2 area. The discs were embedded in Teflon gaskets with provision for electrical connections. The specimens were successively polished with 1/0, 2/0, 3/0 and 4/0 emery papers.

2.2. *Preparation of porous electrodes*

Table 1 gives the characteristics of the electrolytic iron powder. It was reduced at 600° C for 2 h in a hydrogen atmosphere. Two types of electrodes were prepared. Compact sintered electrodes were made by pressing the powders on to a nickel-plated 20 mesh iron net of thickness 0.48 mm by applying a pressure of 3.25 tons cm^{-2} to form a pellet of area 1.54 cm^2. These pellets were sintered in a furnace in the range 700 to 900° C for about 30 to 45 min in a hydrogen atmosphere. Loose sintered electrodes were prepared by using a 10 mesh nickel grid of

0021–891X/87 $03.00 + .12

Table 1. Characteristics of electrolytic iron powder

Chemical composition	99% Fe, 0.01% Pb, 0.008% Zn, 0.001% As, 0.025% Mn, 0.005% Cu
Apparent density[a]	2.8482 g cm^{-3}
Tap density[a]	3.0813 g cm^{-3}
Specific surface area	1.06739 m^2 g^{-1}
Particle size	$< 37\ \mu$m
Predominant phase[b]	α-Fe

[a] From Scott volumeter;
[b] X-ray diffraction.

0.1 mm thickness over which the powder was spread uniformly with a geometric area of 1.67 cm^2. These electrodes were sintered in a furnace in the range 900 to 950° C for about 30 to 45 min in a hydrogen atmosphere. The specific surface area of the powder and pellets and porosity were measured using a mercury penetration porosimeter (Model 910 series, Micromeritics). Table 2 presents the conditions of preparation and characteristics of the porous electrodes. The electrodes were used as prepared without further treatment. The experimental set-up comprised a solid state, low-frequency function generator, potentiostat, x–y–t recorder and digital multimeter [16]. Experiments in duplicate were carried out at 30 ± 0.01° C using Analar chemicals dissolved in doubly distilled water. The solutions were deoxygenated by bubbling purified hydrogen for 1 h. Potentials were measured against Hg/HgO and no corrections were made for liquid junction potentials.

3. Results and discussion

The electrode was kept at −1.3 V for 5 min, disconnected, shaken free of absorbed hydrogen bubbles and polarized to −0.3 V. This potential was fixed after several experiments to get reproducible *E–i* curves for different sweep rates. For solid electrodes, sweep rates of 20–200 mV s^{-1} were used while the maximum sweep rate used for sintered electrodes was 15 mV s^{-1}.

3.1. *Solid electrodes*

The electrochemical spectrum of solid iron has a plateau and two anodic peaks in the forward and two peaks on the reverse scan (Fig. 1). The anodic plateau appears at −970 mV (I) with peaks at −800 mV (II), −575 mV (III) and cathodic peaks at −1000 mV (IV) and −1125 mV (V). On repetitive scanning at higher sweep rates the current flowing under peaks III and IV increases with scan number, suggesting that they are conjugated, while that under peak V decreases. The measurements of anodic peak currents were carried out by measuring currents from the plateau to the peak of the anodic wave. The cathodic peak currents were measured during the reverse scan from the foot of the respective waves.

Table 2. Characterization of porous electrodes

Electrode number	*Sintering variable*			*Thickness (mm)*	*Porosity (%)*	*Specific surface area ($m^2 g^{-1}$)*
	Atmosphere	*Temperature (° C)*	*Time (min)*			
1	N_2	700 ± 10	30	2.0	18.6	0.412
2	N_2	800 ± 10	30	2.1	43.9	0.964
3	N_2	900 ± 10	30	2.1	17.95	0.339
4	N_2	900 ± 10	45	4.3	18.96	0.238
5	H_2	900 ± 10	30	2.0	57.6	–
6	H_2	900 ± 10	45	2.0	55.8	–
7	H_2	950 ± 10	30	2.0	60.1	0.694

Electrodes 1 to 4, green compaction pressure = 3.25 tons cm^{-2}.
Electrodes 5 to 7, loose sintering of iron powders.

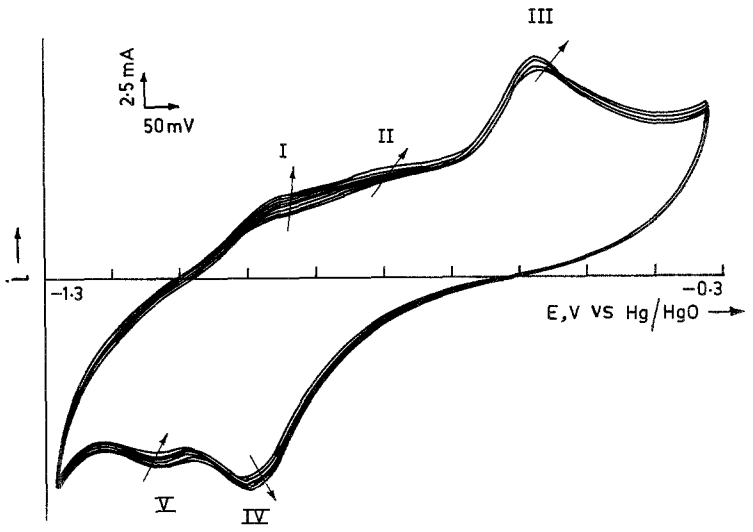

Fig. 1. Typical cyclic voltammogram for solid iron electrode in deoxygenated 6.0 M KOH + 0.63 M LiOH solution. Sweep rate = 200 mV s^{-1}; $E_{\lambda,c}$ = −1.3 V.

The dependence of peak current (i_p) and peak potential (E_p) on sweep rates were studied. The currents observed on cyclic sweeping were of the order of 10 mA cm^{-2} while the double layer charging current, assuming a capacity of 100 μF cm^{-2} over the entire range, was 30 μA cm^{-2}. Hence, the observed currents were principally due to pseudo-capacitative oxide formation and reduction phenomena.

3.1.1. Analysis of plateau current. The plateau current was studied as a function of sweep rate. The values of i_p as well as the charges involved in the oxidation peaks II and III were measured starting from this base line. Various growth laws were involved in the oxidation process. Sato and Cohen [17] proposed a place exchange mechanism for oxide growth in neutral solutions. The film growth proceeds by the field-assisted place exchange of metal oxide pairs. The overall transfer of oxygen (as O^{2-}) from the solution to the outermost lattice layer of metal oxide is considered to take place in two steps.

$$OH^-_{soln} \rightleftharpoons OH^-_{ox} \qquad (1)$$

$$OH^-_{ox} \longrightarrow O^{2-}_{latt} + H^+_{soln} \qquad (2)$$

where $(\ )_{ox}$ represents adsorption at an active site on the oxide. Reaction 2, incorporation into the lattice, is claimed to be rate controlling. Under these conditions the rate of oxide growth is proportional to the total number of surface sites available for OH^- adsorption.

$$i = D\gamma v \qquad (3)$$

there $\gamma = 19.5\,V^{-1}$; v is the scan rate; and D is given by $D = 4neRT/l^2W$, where n is the stoichiometric number which corresponds to the rate determining step, l is the lattice distance of oxygen in a unit cell of the oxide, and W is the activation energy for each metal exchange. For carbon steel in concentration sodium hydroxide below 5 M concentration the dependence of E_p and i_p on sweep rate suggested the possible low field migration of ions through an oxide–hydroxide interface [12].

$$i = \left(\frac{nFk}{V_m}\right)^{1/2} v^{1/2} \qquad (4)$$

where V_m is the molar volume of the film [18]. In the case of low-field ion injection into the film [19–21] is rate determining,

$$i = \left(\frac{6Fa^{1/2}}{V_m}\right)\frac{v}{i^{1/2}} \qquad (5)$$

where a is the half width of the barrier to ion movement. The linear dependence of $i^{3/2}$ versus sweep rate (Fig. 2) suggests that low-field ion injection into the film is the slow step for concentrations above 5 M. However, for sufficiently high potentials and at higher temperatures the high-field mechanism was suggested [11].

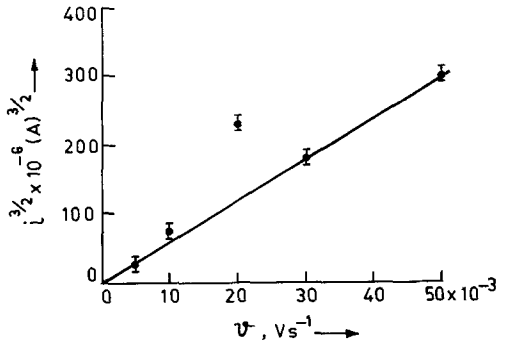

Fig. 2. Plot of $i^{3/2}$ versus sweep rate for plateau current in 6.0 M KOH + 0.63 M LiOH solution.

3.1.2. Analysis of peaks II and III. Table 3 presents the possible oxidation–reduction schemes and associated equilibrium potentials [22]. The oxidation–reduction process may involve overpotentials and a necessary condition for an oxidation to take place is $E_{p,a} > E_e$ at potentials noble to E_e. Similarly, a reduction process can occur at potentials negative to $E_e (E_{p,c} > E_e)$.

$$Fe + 2H_2O \rightleftharpoons Fe(OH)_2 + 2H^+ + 2e \quad (6)$$

$$E_e = -0.047 - 0.0591 \text{ pH at } 25°C$$

$$Fe(OH)_2 \rightleftharpoons FeOOH + H^+ + e \quad (7)$$

$$E_e = 0.271 - 0.591 \text{ pH at } 25°C$$

$$3Fe(OH)_2 \rightleftharpoons Fe_3O_4 + 2H_2O + 2H^+ + 2e \quad (8)$$

$$E_e = -0.202 + 0.0591 \text{ pH at } 25°C$$

The potential difference is +318 mV for FeOOH and −155 mV for Fe_3O_4 at constant pH and temperature. The observed potential difference between E_p(II) and E_p(III) is due to the change in OH^- ion activity of the electrode due to potential sweeping; hence, it is due to the conversion of $Fe(OH)_2$ to FeOOH. The occurrence of peaks at −800 mV and −575 mV is due to the formation of $Fe(OH)_2$ and FeOOH, respectively, and the cathodic peak is due to the reduction of $Fe(OH)_3$/FeOOH to $Fe(OH)_2$ which can dissolve in higher alkali concentration. The dissolution of the oxide or the underlying metal by the ion transport through the oxide can also take place.

A plot of E_p(II) versus log v gave a slope of 30 mV and (d log i_p/d log v) = 0.5. This indicates the adsorption of hydroxyl ion with monolayer coverage on the oxide or uncovered metal surface [23]. A clear surface was never exposed to the solution phase and, over a partially oxidized surface, adsorption takes place. The fractional dependence for (d log i_p/d log v) indicates that diffusion in the solid state or oxide zone can take place. It was proposed earlier [10] that

$$Fe + OH^- \rightleftharpoons [Fe(OH)]_{ad} + e \quad (9)$$

$$[Fe(OH)]_{ad} \longrightarrow [Fe(OH)]^+_{ad} + e \quad (10)$$

$$[Fe(OH)]^+_{ad} + OH^- \rightleftharpoons Fe(OH)_2 \quad (11)$$

At high temperatures

$$[Fe(OH)]^+_{ad} + 2OH^- \longrightarrow HFeO_2^- + H_2O \quad (12)$$

At higher anodic potentials $Fe(OH)_2$ can react with OH^- to form FeOOH

$$Fe(OH)_2 + OH^- \rightleftharpoons FeOOH + H_2O + e \quad (13)$$

Table 3. Possible oxidation–reduction schemes and associated equilibrium potentials (mV vs Hg/HgO) at 30° C and pH 15

Number	*Reactions*	E *(mV)*
1	$3HFeO_2^- + H^+ \rightleftharpoons Fe_3O_4 + 2H_2O + 2e$	−1479
2	$3Fe(OH)_2 + H_2O \rightleftharpoons Fe_3O_4 + 2H^+ + 2e$	−1182
3	$3Fe + 4H_2O \rightleftharpoons Fe_3O_4 + 8H^+ + 8e$	−1065
4	$Fe + 2H_2O \rightleftharpoons Fe(OH)_2 + 2H^+ + 2e$	−1025
5	$Fe + 3H_2O \rightleftharpoons Fe(OH)_3 + 2H^+ + 2e$	−951
6	$Fe + 2H_2O \rightleftharpoons HFeO_2^- + 3H^+ + 2e$	−949
7	$Fe(OH)_2 + H_2O \rightleftharpoons Fe(OH)_3 + H^+ + e$	−1023

The direct oxidation of Fe to FeOOH may also follow the same sequence. FeOOH can dissolve in 6.0 M KOH solutions to yield Fe(III) species of $HFeO_2^-$. The $HFeO_2^-$ species formed in the solution can also undergo oxidation.

$$HFeO_2^- \rightleftharpoons FeO_2^- + H^+ + e \quad (14)$$

or

$$FeOOH + OH^- \rightleftharpoons FeO_2^- + H_2O \quad (15)$$

$$HFeO_2^- + 2FeO_2^- + H_2O \rightleftharpoons Fe_3O_4 + 3OH^- \quad (16)$$

or

$$2[FeOOH] \longrightarrow [Fe_2O_3 \cdot H_2O] \quad (17)$$

3.2. *Porous electrodes*

Fig. 3 shows the electrochemical spectrum for a porous iron electrode in 6.0 M KOH solution. The forward scan revealed a plateau around −975 mV (I), peaks at −750 mV (II) and −585 mV (III) and in the backward scan a peak at −985 mV (IV) and −1175 mV (V) appeared. On subsequent sweeping the charge under peaks II, III, IV, and V increased, suggesting the reactions are occurring in sequence. Increase of scan number shifted the peak potentials of II and III in the noble direction while the peak potentials of IV and V shifted towards more negative potentials, suggesting that the reactions were becoming irreversible with subsequent sweeping. During the forward sweep iron is oxidized to $Fe(OH)_2$ and to FeOOH and in the backward scan FeOOH is reduced either as $HFeO_2^-$ or $Fe(OH)_2$ and finally to iron. Direct reduction of FeOOH or Fe_3O_4 to iron can also occur at more negative potentials.

3.3. *Effect of addition agents in solutions*

3.3.1. Lithium hydroxide. In 6.0 M KOH solution containing 0.63 M LiOH (Fig. 4) the forward scan revealed a plateau around −970 mV (I) followed by two peaks at −775 mV (II) and −615 mV (III), respectively, while the reverse scan showed three peaks at −1000 mV (IV), −1075 mV (V) and −1190 mV (VI), respectively. On repetitive scanning the current flowing under the peaks increased showing that the reactions are occurring in sequence. Increase of the concentration lithium ion (0.21 to 0.84 M) caused the anodic peaks II and III to appear at less negative potentials, thereby favouring the $Fe(OH)_2$ and FeOOH formation. The lithium ion is probably incorporated into the oxide lattice via the defect structure and allows easier film growth. The presence of lithium was found to give rise to the formation of magnetite as a clearly identifiable phase after continued cycling [6]. The cathodic peak potentials IV and V were shifted to more positive values on cycling. FeOOH may undergo direct reduction to iron

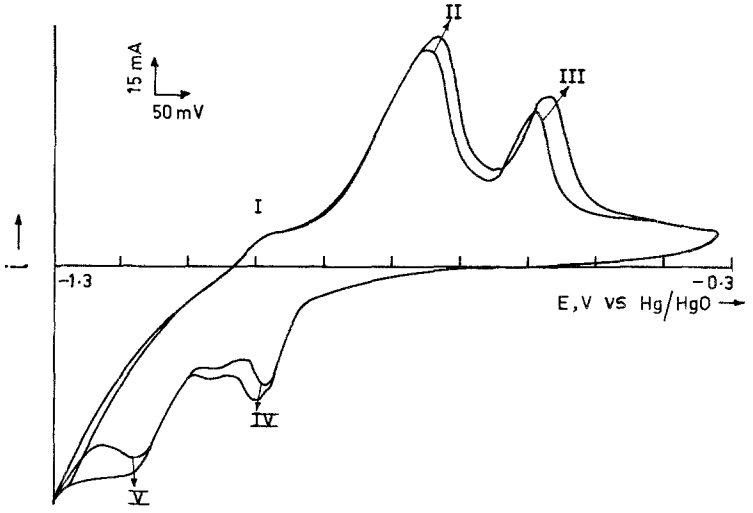

Fig. 3. Typical cyclic voltammogram for porous iron electrode (number 7) in deoxygenated 6.0 M KOH solution. Sweep rate = 2 mV s^{-1}; $E_{\lambda,c}$ = −1.3 V.

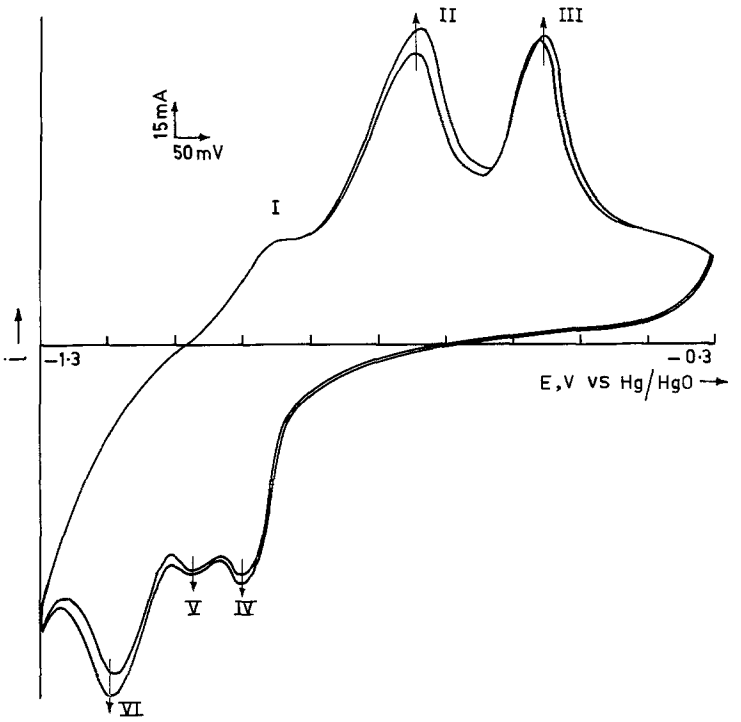

Fig. 4. Typical cyclic voltammogram for porous iron electrode (number 7) in deoxygenated 6.0 M KOH + 0.63 M LiOH solution. Sweep rate = 5 mV s^{-1}; $E_{\lambda,c} = -1.3$ V.

along with the formation of $Fe(OH)_2$. This reduction to metallic iron may take place at -1000 mV. $Fe(OH)_2$ or $HFeO_2^-$ may be completely reduced to iron at -1190 mV. The peak potential separation between the II and V and III and IV couples was reduced considerably with increase in lithium ion concentration.

3.3.2. Additions of sulphur and sulphides. Various amounts of elemental sulphur (10^{-6} to 10^{-3} M), sodium sulphide (10^{-5} to 10^{-2} M), and ferrous sulphides (10^{-7} to 10^{-4} M) were added to 6.0 M KOH solutions. In 10^{-3} M sulphur solution, polarization from -1.3 to -0.3 V revealed a single anodic peak at -590 mV and a cathodic peak at -1.2 V in the reverse scan. Increase of scan number increased the overpotentials for oxidation while the cathodic peak potential was unaffected. Decrease of concentration shifted the anodic peak to less negative values while the cathodic peak potential was unaffected. Adsorption of sulphur atoms [24] alters the interfacial potential as indicated by the shifting of zero current potentials to more noble values. Trivalent iron may be formed via $Fe(OH)_2$ or $HFeO_2^-$ whose formation is hindered by adsorbed sulphur. The increase in overpotentials in subsequent sweeping may be due to the non-availability of $HFeO_2^-$ which diffuses away from the electrode. In 10^{-2} M sodium sulphide solution (Fig. 5) the forward scan revealed a plateau followed by anodic peaks at -675 mV (II) and -400 mV (III) while the reverse scan exhibits a single cathodic peak at -1150 mV (IV). On subsequent cycling the charges under the peaks increased and at higher sweep rates (> 5 mV s^{-1}) single anodic and cathodic peaks appeared indicating that Fe(III) was directly reduced to iron. Addition of sodium sulphide increases the overpotential of formation of ferrous and ferric oxides and decreases the reduction overpotential of ferric iron. The presence of sulphide reduces the rate of oxide film thickening. Sulphide ion interacts strongly with Fe^{2+} or Fe^{3+} in the oxide film and slows down the hydroxide formation as indicated by large overpotentials compared to the absence of sulphide ion. In dilute alkaline sulphide solutions [15] formation of sodium ferric sulphide was identified and the oxidation of the sulphide ion leads to repassivation of the electrode by elemental sulphur. The dissolution as $HFeO_2^-$ is favoured in the presence of sulphide

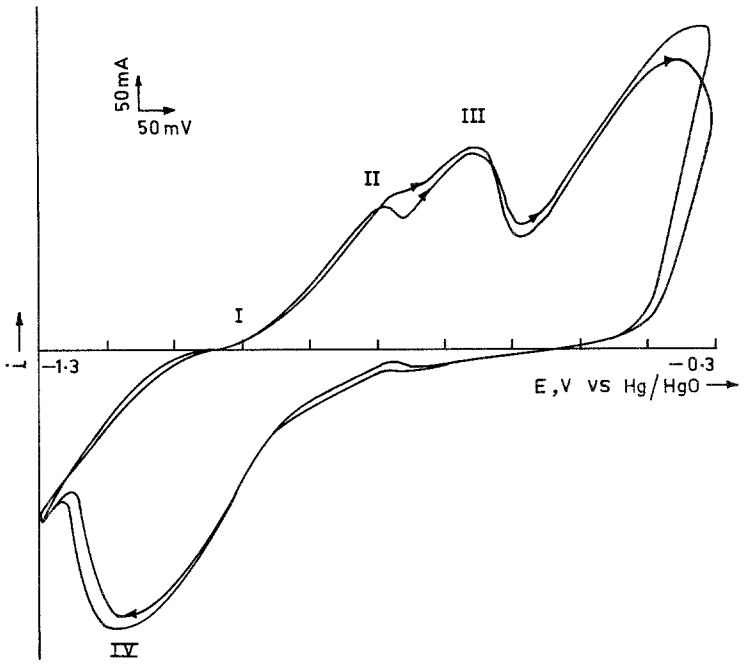

Fig. 5. Typical cyclic voltammogram for porous iron electrode (number 7) in deoxygenated 6.0 M KOH + 10^{-2} M Na_2S solution. Sweep rate = 2 mV s^{-1}; $E_{\lambda,c}$ = −1.3 V.

ions forming a soluble ferrous complex or, on further oxidation, a soluble ferric sulphide complex. The cathodic peak potential appeared positive to the equilibrium potential of FeOOH/$Fe(OH)_2$ suggesting that the reduction of Fe(III) to the soluble ferrous ion is favoured. The formation of K_2FeS_2 and $KFeS_2$ is possible during oxidation. At higher potentials, greater than −600 mV, the formation of polysulphides via the decomposition of $KFeS_2$ is possible. In 10^6 M FeS in 6.0 M KOH solution, polarization from −1.3 to −0.3 V revealed the zero crossing potential at −1015 mV followed by a plateau around −800 mV and an anodic peak at −460 mV. In the reverse scan at −1075 mV and −1175 mV, two cathodic peaks appeared. On subsequent sweeping the zero current potential shifted to more positive values and the anodic peak potential to less positive values. Thickening of the film took place with subsequent cycling. At potentials greater than −400 mV further increase in current was observed due to the oxidation of soluble species. Addition of ferrous sulphide does not favour the FeOOH/$Fe(OH)_2$ reaction while the formation of soluble ferrous sulphide and ferric sulphide were favoured. Increase in the concentration of ferrous sulphide favoured the formation of soluble species as evidenced by greater current flow. The dissolution of ferric oxide or hydroxide is likely to take place as

$$Fe^{3+} + 2S^{2-}_{ads} \rightleftharpoons FeS^{-}_{2_{ads}} \qquad (18)$$

The soluble ferric sulphide complex undergoes polymerization accompanied by precipitation with K^+ ions.

$$nFeS_2^- \longrightarrow (FeS_2)_n^{n-} \qquad (19)$$

$$nK^+ + (FeS_2)_n^{n-} \longrightarrow (KFeS_2)_n \qquad (20)$$

The $KFeS_2$ undergoes reduction to the soluble ferrous ion during the backward scan and is further reduced to metallic iron. At higher anodic potentials polysulphide formation is possible as suggested earlier [15].

3.3.3. Addition of trivalent oxides. Various amounts of As_2O_3 (10^{-6} to 10^{-3} M) and Sb_2O_3 (10^{-7} to 10^{-4} M) were added to 6.0 M KOH solutions. Excursions from −1.3 to −0.3 V in 10^{-3} M arsenite revealed an anodic peak at −650 mV while the reverse scan exhibited a single cathodic peak. On subsequent cycling the anodic peak potential shifted to more positive values while the cathodic peak potential was unaffected. The charges under the peaks increased with increase in scan number,

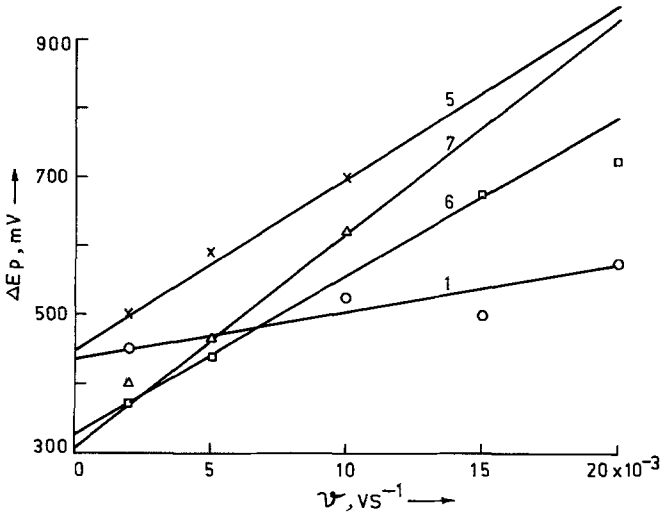

Fig. 6. Plot of ΔE_p versus sweep rate for Fe/Fe(II) couple in 6.0 M KOH + 0.63 M LiOH solution.

suggesting both reactions are coupled. Iron may be oxidized directly to FeOOH either through $Fe(OH)_2$ or $HFeO_2^-$. During the forward scan in 10^{-6} M antimonate solution the zero current potential occurred at -1050 mV followed by a plateau around -850 mV and an anodic peak at -650 mV. The reverse scan exhibited a single cathodic peak at -1225 mV. On subsequent cycling the anodic peak potential shifted to more positive values while the cathodic peak potential was unaffected. On cycling, the charges under the peaks decreased suggesting the species which undergo oxidation and reduction diminish with time. The dissolved $HFeO_2^-$ diffuses away from the electrode, thereby decreasing Q_a and Q_c. Antimonate increased the overpotential of the anodic process, favouring reductive dissolution as $HFeO_2^-$ by adsorption on the surface.

4. Criteria for the battery electrode

An ideal reversible battery requires that the positive and negative electrodes be electrodes of the second kind [25], i.e. a metal in contact with its sparingly soluble salt and solution saturated with the salt.

$$O_s + X + ne \rightleftharpoons R_s + Y \qquad (21)$$

O_s and R_s are oxidant and reductant present in the solid phase and the species X and Y are species from the electrolyte. The process

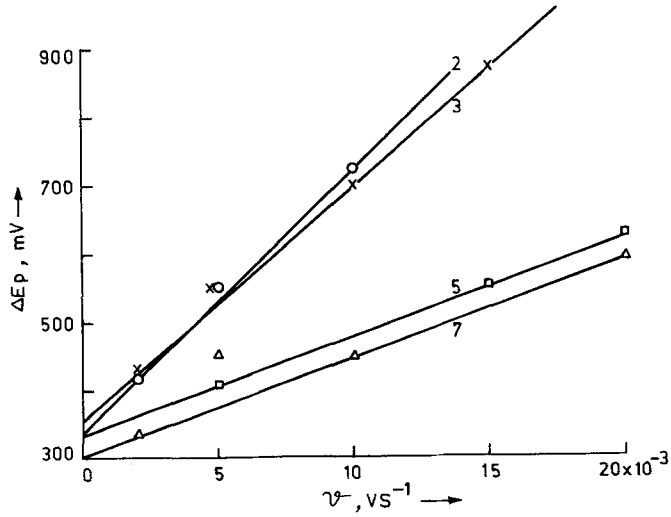

Fig. 7. Plot of ΔE_p versus sweep rate for Fe(II)/Fe(III) couple in 6.0 M KOH + 0.63 M LiOH solution.

Table 4. Parameters obtained from cyclic voltammograms in 6.0 M KOH + 0.63 M LiOH solution

Number	*Fe/Fe(II) couple*		*Fe(II)/Fe(III) couple*	
	$(\Delta E_p)_{v=0}$	$(Q_c/Q_a)_{v=0}$	$(\Delta E_p)_{v=0}$	$(Q_c/Q_a)_{v=0}$
Solid electrode	275	0.74	305	0.89
1	435	0.58	410	0.83
2	325	0.77	340	0.55
3	350	0.53	355	0.67
4	–	0.28	650	0.32
5	450	0.33	335	0.63
6	325	0.83	450	0.54
7	310	0.68	305	0.75

involves dissolution from kink sites and deposition by nucleation of the active materials in the oxidized and reduced forms of the solid phase. In the case of iron electrodes, dissolution can occur through the oxide layer or the oxide itself dissolves to yield soluble species such as $HFeO_2^-$. The oxide film thickness increases with increase in the electrode potential. This explains the appearance of a plateau current in the cyclic voltammograms.

The appearance of an anodic peak potential (II) and the cathodic peak potential (V) corresponds to the Fe/Fe(II) redox couple.

$$(E_{p(II)} - E_e) - (E_{p(V)} - E_e) = \Delta E_p \qquad (22)$$

is the measure of the irreversibility. The greater the value of ΔE_p the more irreversible is the electrode process. Since ΔE_p varies linearly with sweep rate, $(\Delta E_p)_{v=0}$ is used to evaluate the electrode for reversibility. A similar procedure was followed for $E_{p(III)} - E_{p(IV)} = \Delta E_p$ for the Fe(II)/Fe(III) redox couple. Figs 6 and 7 show the ΔE_p versus sweep rate plot for different electrodes. Even for solid electrodes, $(\Delta E_p)_{v=0}$ for the Fe/Fe(II) couple and Fe(II)/Fe(III) couple are 275 mV and 305 mV respectively. An electrode which gives $(\Delta E_p)_{v=0}$ values closer to the solid electrode is considered to be the best electrode. It may be seen from Table 4 that the electrodes 6 and 7 give values closer to the solid electrode.

For an ideally reversible case, $(Q_c/Q_a) = 1$. As (Q_c/Q_a) varies with sweep rate, $(Q_c/Q_a)_{v=0}$ is taken as a measure of the reversibility (Figs 8, 9). For a solid electrode, the values of $(Q_c/Q_a)_{v=0}$ for the Fe/Fe(II) and Fe(II)/Fe(III) couples are

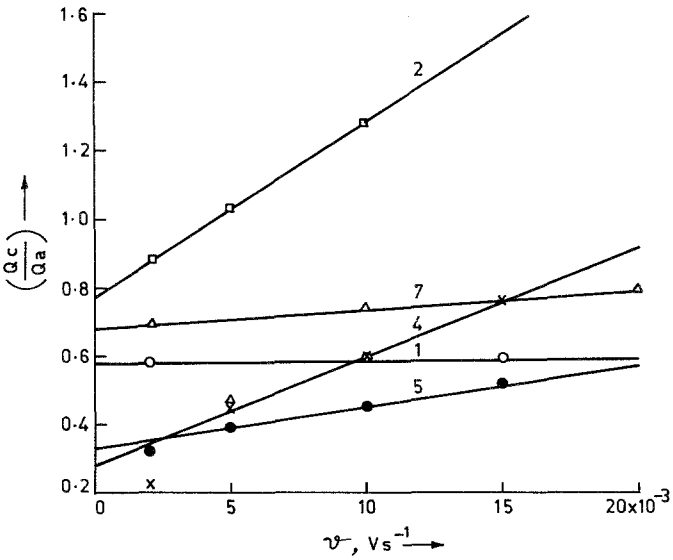

Fig. 8. Plot of (Q_c/Q_a) versus sweep rate for Fe/Fe(II) couple in 6.0 M KOH + 0.63 M LiOH solution.

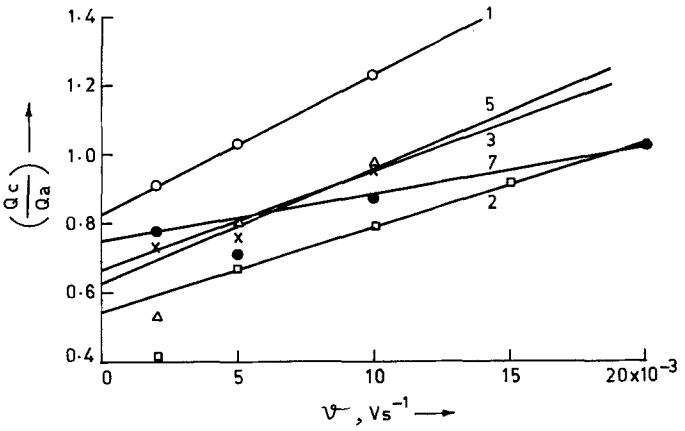

Fig. 9. Plot of (Q_c/Q_a) versus sweep rate for Fe(II)/Fe(III) couple in 6.0 M KOH + 0.63 M LiOH solution.

0.74 and 0.89 respectively. The electrodes 6 and 7 give values closer to that of the solid electrode. The values of $(\Delta E_p)_{v=0}$ for the Fe/Fe(II) and Fe(II)/Fe(III) couples suggests that the electrode prepared by loose sintering at 900 and 950° C in a hydrogen atmosphere is suitable as a battery electrode.

References

[1] T. K. Teplurskaya, N. N. Fedorova and S. A. Rozentsveig, *Zh. Fiz. Khim.* **38** (1964) 2167.

[2] A. J. Salkind, C. J. Venuto and S. U. Falk. *J. Electrochem. Soc.* **111** (1964) 493.

[3] H. G. Silver and E. Leaks, *ibid.* **117** (1970) 5.

[4] L. Ojefors, *ibid.* **123** (1976) 1691.

[5] A. M. Pritchard and B. J. Mould, *Corros. Sci.* **11** (1971) 1.

[6] Y. Geronov, I. Tomov and S. Georgiev, *J. Appl. Electrochem.* **5** (1975) 351.

[7] R. D. Armstrong and I. Baurhoo, *J. Electroanal. Chem.* **34** (1972) 41.

[8] *Idem, ibid.* **40** (1972) 325.

[9] B. O. Andersson and Lars Ojefors, *J. Electrochem. Soc.* **123** (1976) 824.

[10] V. S. Muralidharan and M. Veerashanmugamani, *J. Appl. Electrochem.* **15** (1985) 675.

[11] A. Wieckowski and E. Ghali, *Electrochim. Acta.* **30** (1985) 1423.

[12] D. D. Macdonald and B. Roberts, *ibid.* **23** (1978) 781.

[13] N. A. Hampson, R. J. Latham, A. Marshall and R. D. Gills *ibid.* **19** (1974) 397.

[14] D. S. Poa, J. F. Miller and N. P. Yao, Proc. 166th Meeting, Electrochem. Soc. Abstract 98, Vol. 84-2 (1984) p. 144.

[15] D. W. Shoesmith, P. Taylor, M. G. Bailey and B. Ikeda, *Electrochim. Acta* **23** (1978) 903.

[16] V. S. Muralidharan, K. Thangavel and K. S. Rajagopalan, *ibid* **28** (1983) 1611.

[17] N. Sato and M. Cohen, *J. Electrochem. Soc.* **111** (1964) 512, 519.

[18] D. E. Williams and G. A. Wright, *Electrochim. Acta* **21** (1976) 1009.

[19] T. P. Hoar, *Mod. Asp. Electrochem.* **2** (1959) 262.

[20] A. J. Fromhold, Jr, 'Oxides and Oxide Films', Vol. 3 (edited by J. W. Diggle and A. K. Vijh), Marcel Dekker, New York (1976).

[21] A. J. Fromhold, Jr, 'Theory of Metal Oxidation', Vol. 1, North-Holland, Amsterdam (1976).

[22] M. Pourbaix, 'Atlas of Electrochemical Equilibria in Aqueous Solutions', Pergamon Press (1966).

[23] S. Srinivasan and E. Gileadi, *Electrochim. Acta* **11** (1966) 321.

[24] Von. H. Kaesche, *Werkstoffe und Korrosion* **21** (1970) 185.

[25] S. Sathyanarayana, *Trans. SAEST* **11** (1976) 19.